Journal of Alloys and Compounds 513 (2012) 68–74

Contents lists available at SciVerse ScienceDirect

Journal of Alloys and Compounds

journal homepage: www.elsevier.com/locate/jallcom

Characteristics of Cu(In,Ga)Se_2 (CIGS) thin films deposited by a direct solution coating process

MyoungGuk Park[a], SeJin Ahn[a,*], Jae Ho Yun[a], Jihye Gwak[a], Ara Cho[a], SeoungKyu Ahn[a], Keeshik Shin[a], Dahyun Nam[b], Hyeonsik Cheong[b], Kyunghoon Yoon[a]

[a] Photovoltaic Center, Korea Institute of Energy Research, 71-2 JangDong, YuseongGu, DaeJeon 305-343, Republic of Korea
[b] Department of Physics, Sogang University, Seoul 121-742, Republic of Korea

ARTICLE INFO

Article history:
Received 8 August 2011
Received in revised form 8 September 2011
Accepted 8 September 2011
Available online 4 October 2011

Keywords:
Solar cells
Thin film
CIGS
Non-vacuum
Solution

ABSTRACT

Cu(In,Ga)Se_2 (CIGS) thin films were formed by a direct non-vacuum coating and a subsequent selenization of low cost precursor solutions, and their compositional, structural and optical properties were characterized. Selenized films showed a double-layered structure with an upper layer of chalcopyrite CIGS and an amorphous bottom layer mainly composed of carbon. For the upper CIGS layer, good compositional controllability for Cu and Ga was confirmed by linear relationship between metal ratios of the precursor solution and those of the selenized films. Effects of Cu and Ga contents on structural and optical properties of the films were also characterized by X-ray diffraction (XRD), Raman and photoluminescence (PL) analyses, and the results were interpreted by defect supercluster formation (V_{Cu}–In_{Cu}) in Cu-deficient films and mass and size difference between In and Ga, respectively. Further, the bottom layer was found to be mostly composed of conductive amorphous carbon, which is the main current flow path in the completed solar cells.

© 2011 Elsevier B.V. All rights reserved.

1. Introduction

Chalcopyrite Cu(In,Ga)Se_2 (CIGS) compound is a direct band-gap material and has a light absorption coefficient higher than 10^5 cm^{-1}. These inherent material properties, in conjunction with its tunable band-gap and thermal and chemical stability, lead CIGS to be one of the most promising absorber materials for thin film solar cells. The best CIGS thin film solar cell has already reached a confirmed conversion efficiency of about 20% [1]. However, in spite of the high efficiency of state-of-the-art CIGS solar cells, the high production cost of conventional vacuum-based processes, i.e., a multi stage co-evaporation and a two-step process of sputtering and selenization, is considered to be a main obstacle to the widespread use of CIGS thin films solar cells [2].

In this regard, many efforts have been devoted to develop alternative deposition techniques for thin film CIGS solar cells using non-vacuum coating processes [2–14], based on their inherent advantages such as no requirement of expensive vacuum equipments, less energy intensive deposition and much better material utilization. These non-vacuum coating processes can be roughly divided into two categories depending on precursor types, in which the first approach uses the true solution precursors [3–7] and the other uses particulate precursors [2,8–14]. Potential of the solution precursor approach as a more cost-effective method than the particle-based one was demonstrated previously [7], in that the solution precursors with proper rheology can be directly coated on a substrate and hence the number of processing steps can be reduced.

Among the solution coating approaches, the highest efficiency achieved to date is 12.3% by hydrazine based method in which hydrazine was used as a solvent for dissolving metal chalcogenides to fabricate CIGS absorber layer [4]. Although their result showed a noticeable cell efficiency with a dense CIGS absorber layer comparable to that produced by a vacuum-based deposition, the use of highly toxic and explosive hydrazine is considered to be a hurdle for commercial utilization.

On the other hand, Kaelin et al. [6] and Ahn et al. [7] reported a solution based process in which the most cost-effective and environmentally friendly combinations of starting chemicals (metal-nitrates and -chlorides), solvents (basic alcohols) and heat treatment medium (Se vapor) were used. By this method, a remarkably high efficiency of 6.7% was obtained for a CIGS thin film solar cell [6]. It is more surprising that they obtained the efficiency with a double layered absorber film with a top CIGS layer and a thick bottom layer of residual carbon, reflecting that the carbon layer is not a perfectly insulating layer. However, they did not perform sophisticated investigations on the electro-optical properties of the top CIGS layer and the mechanism of current path through the thick

* Corresponding author. Tel.: +82 42 860 3541; fax: +82 42 860 3739.
E-mail address: swisstel@kier.re.kr (S. Ahn).

0925-8388/$ – see front matter © 2011 Elsevier B.V. All rights reserved.
doi:10.1016/j.jallcom.2011.09.080

carbon layer. In other words, it is prerequisite for further improving the performance of the device to understand the physicochemical properties of the CIGS layer, especially the property changes of the films with their compositional variation such as Cu/III and Ga/III ratios, and the structure of the residual carbon layer.

In this paper, we report the characteristics of CIGS layers prepared by a direct solution coating process, focusing on the controllability of film compositions and the compositional effects on the film properties. In addition, the result of compositional study on the residual carbon layer is presented to elucidate and suggest a possible current path through it.

2. Experimental

2.1. Reagents

Copper nitrate hydrate ($Cu(NO_3)_2{\cdot}3H_2O$; 99.999%), indium chloride ($InCl_3$; 99.999%) and gallium nitrate hydrate ($Ga(NO_3)_3{\cdot}H_2O$; 99.9%) were purchased from Sigma Aldrich, methanol (CH_3OH, 99.6%) from Junsei, elemental Se (99.999%, 3 mm shot) from Cerac and ethyl-cellulose (EC, 90–110 mPa s) from Kanto Chemical Co. $Cu(NO_3)_2$, $InCl_3$ and $Ga(NO_3)_3$ were stored in a nitrogen filled glove box to prevent air or humidity induced degradation.

2.2. Preparation of precursor solution

1 g of copper nitrate, 0.66 g of indium chloride and 0.35 g of gallium nitrate were dissolved in 20 ml of methanol. In this case, the metal ratios are Cu/III = 1 and Ga/III = 0.3, respectively, in the solution. The metal ratios were able to be modified simply by changing the amount of starting chemicals dissolved in the solution. To adjust the viscosity of the precursor solution to be suitable for doctor blade coating, 6 g of ethyl-cellulose (EC) was dissolved in 40 ml of methanol, and this viscous solution was mixed with the Cu-, In- and Ga-containing methanol solution mentioned above. The final mixture was stirred with a magnetic bar vigorously for 1 h. All the preparation processes were performed at room temperature in air.

2.3. Thin film deposition and selenization

Precursor films were deposited on a Mo-coated sodalime glass by the doctor blade coating (Multi coater, DCN Co. Ltd, Korea). The samples were then dried at 80 °C for 5 min in air on a hot plate to evaporate methanol. Selenization was performed in a vacuum evaporator equipped with a Knudsen-type effusion cell. Initially the chamber was evacuated to a base pressure of 5×10^{-6} Torr with a turbo molecular pump and then elemental Se was evaporated from the effusion cell. Typical substrate temperature and selenization time were 530 °C and 30 min, respectively. The flux of Se vapor was regulated by the effusion cell temperature.

2.4. Characterization of thin films

Morphologies and compositions of the precursor films and the selenized films were investigated by the high-resolution scanning electron microscopy (HRSEM, XL30SFEG Phillips Co., Holland at 10 kV) and the Energy Dispersive Spectroscopy (EDS, EDAX Genesis apex, acceleration voltage: 30 kV, collection time: 100 s with standard-less method), respectively. The crystalline structure of the films was identified by the X-ray diffraction (XRD, Rigaku Japan, D/MAX-2500) using Cu Kα line and the Raman spectroscopy. The Raman spectra were taken in the quasi-backscattering geometry by using the 514.5 nm line of an Ar ion laser as the excitation source. The scattered light was filtered with a holographic edge filter and dispersed by a Spex 0.55-m spectrometer and detected with a liquid-nitrogen-cooled back-illuminated charge-coupled-device (CCD) detector array.

PL was used to investigate the optical properties of CIGS films. PL measurements were performed in a closed-cycle helium refrigerator system at 10 K. The 514.5-nm line of an Ar-ion laser was used was the excitation source. The luminescence signal was dispersed by a SPEX 0.55 m spectrometer and detected with a strained-InGaAs photodiode for infrared region.

Depth compositional profile of the selenized film was obtained by the Auger electron spectroscopy (AES, PerkinElmer, SAM 4300).

3. Results and discussion

3.1. A Typical example of double-layered CIGS/carbon films

Fig. 1(a) shows a typical SEM image of the precursor film. A uniform and crack-free film of 8.6 μm in thickness was formed, which consisted of CuCl crystals (Fig. 1(b)) and amorphous In and Ga compounds embedded in EC matrix. The presence of In and Ga was confirmed by EDS analysis (not shown here).

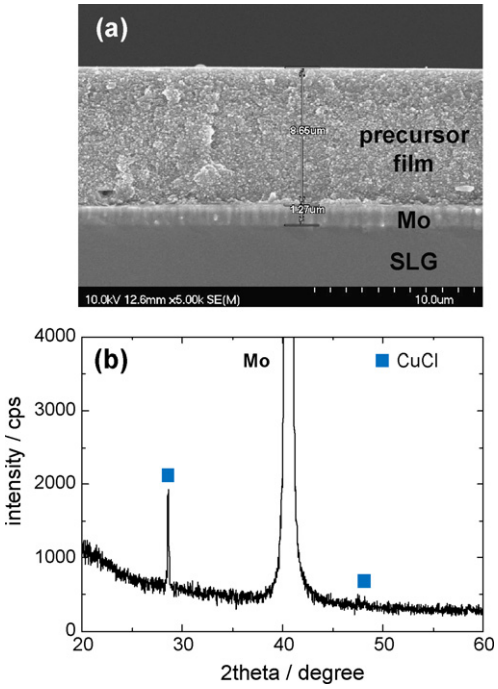

Fig. 1. (a) Cross-sectional SEM picture and (b) XRD patterns of the precursor film.

A typical SEM micrograph of the final film selenized at 530 °C for 30 min with Se vapor was presented in Fig. 2(a), showing that the total thickness of selenized film was reduced to about 3 μm and had a double-layered structure with a 800 nm thick upper layer, which appears to be dense, flat and well crystallized and a 2.2 μm thick amorphous-like bottom layer. From the XRD pattern (Fig. 2(b)) and the AES depth profile (Fig. 2(c)), it was found that the upper layer was a chalcopyrite CIGS with a strong (1 1 2) preferred orientation, and the bottom layer mainly composed of residual carbon.

From Fig. 2, the topics to be addressed in this paper can be clarified again as follows;

(1) Controllability of the composition of CIGS layer, i.e., how well the Cu/III and Ga/III ratios of the starting solutions transfer to those of the final films.
(2) Effects of Cu/III and Ga/III ratios on the structural and optical properties of CIGS layer.
(3) How electrical current flows through such a thick residual carbon layer, as demonstrated by Kealin et al. [6] and Ahn et al. [7]. More concretely, whether the current flows by a conductive path embedded in carbon matrix possibly formed by a connection of unreacted source materials, i.e., CuCl, In or Se as suggested by Ahn et al. [7] or the cabon itself, in any conductive form, acts as a conductive path.

3.2. Controllability of composition of CIGS films

The controllability of composition is an important issue in the fabrication of CIGS by solution process because it has been often reported that there was significant difference between the composition of the precursors and the final films [7,15–17]. In this regard, we investigated the change in the compositional ratios of major metals (Cu and Ga) after selenization, and the results are presented in Fig. 3. For a comparison, Cu/In ratios of CIS films prepared by the same approach as that used in this work, reported by Ahn et al. [7], are shown together in Fig. 3(a) as red circles.

Generally, Cu/III and Ga/III ratios of the selenized films show good linearity with those of the precursor solutions in spite of

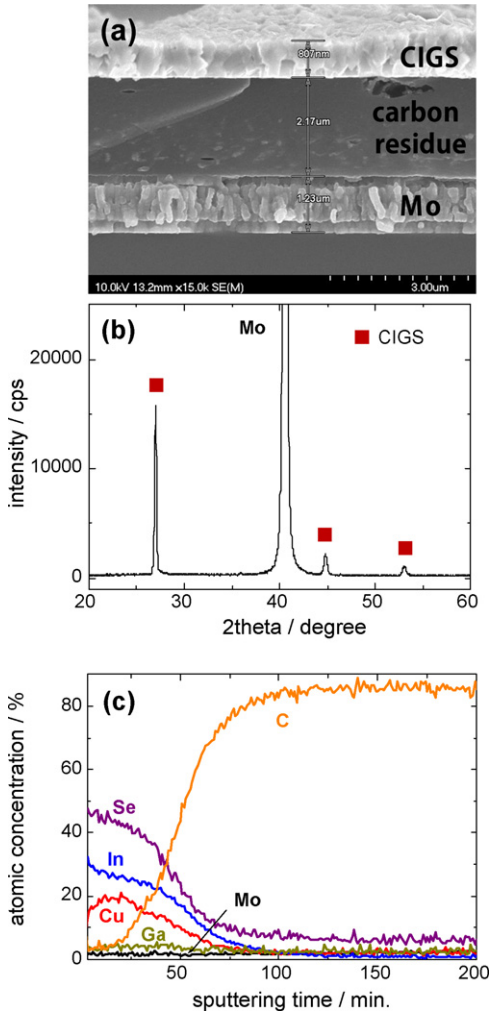

Fig. 2. (a) Cross-sectional SEM picture, (b) XRD pattern and (c) AES depth profile of the selenized film.

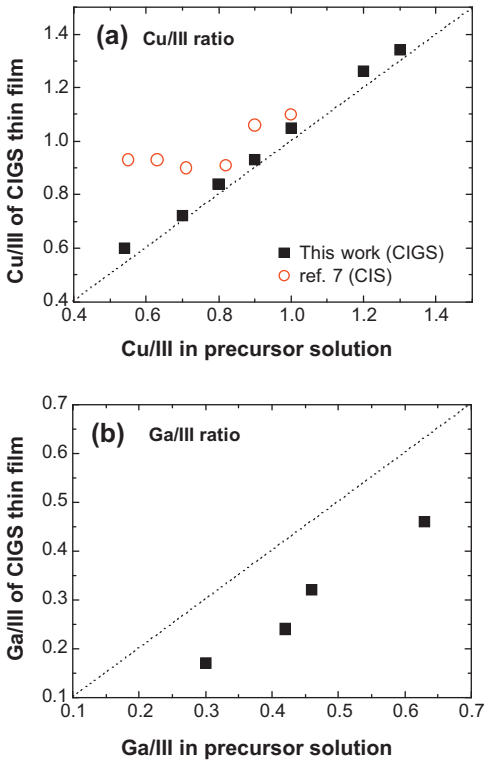

Fig. 3. Relationship between the compositions of the precursor solutions and that of the final CIGS thin films; (a) Cu/III ratios and (b) Ga/III ratios. Red circles in (a) represents the Cu/In ratios of CIS from Ahn et al. [7]. (For interpretation of the references to color in this figure legend, the reader is referred to the web version of the article.)

slight increase in the absolute values of Cu/III (Fig. 3(a)) and decrease of Ga/III (Fig. 3(b)). This linearity was not observed in the case of CIS (red circles in Fig. 3(a)), in which the minimum achievable Cu/III (=Cu/In) ratio of films was 0.9 with starting solution of Cu/In = 0.8, and further dose of In was not effective in decreasing the Cu/In ratio of the CIS films [7]. This result implies that the controllability is affected by the addition of Ga.

It was previously reported that In and Ga loss can occur by evolution of volatile In_2Se [18,19] and Ga_2Se [19,20], respectively, when supply of Se or Se overpressure is insufficient during selenization. The Cu/In ratios of final CIS films shown in Fig. 3(a) was also attributed to significant evaporation of In_2Se from the sample, confirmed by the effects of Se flux and substrate temperature on Cu/In ratios of final films [7].

Thus, it is rational to consider that there should be a competition between the evaporation of In_2Se and Ga_2Se gases during the selenization process of this work, which is expected to be determined by following two factors; firstly, it will be affected by the difference in vapor pressures of those two species. However, a simple comparison of vapor pressures is insufficient for explaining the phenomena, because there is a significant difference in the rate of reactions leading to the formation of Cu–III–Se_2, which is the second factor. The latter is related to the possibility to form III_2–Se vapor itself because the element with higher reaction rate to form Cu–III–Se_2 definitely has lower possibility to be evaporated from the sample.

Unfortunately, a direct comparison of vapor pressures of those two species was not possible due to lack of reports on the quantitative values of vapor pressures especially of Ga_2Se. Piacente et al. [21] reported vapor pressure of Ga_2Se gas over solid Ga_2Se_2 in the temperature range between 770 and 950 °C, but the temperature is too high to be directly compared with vapor pressure of In_2Se gas measured under 440 °C by Greenberg [22]. Thus, an indirect comparison was performed by extrapolating each $-\log_{10}(p(III_2Se))$ vs. $1/T$ curves to near 530 °C, resulting that vapor pressure of In_2Se is significantly higher than that of Ga_2Se by several orders of magnitude. This means that the difference in vapor pressure of III_2–Se gas may not be a reason for the Ga loss during selenization in this work (Fig. 3(b)) in spite of apparently large uncertainties involved in the above calculation.

On the other hand, the reaction rate of the formation of $CuInSe_2$ is reported to be higher in magnitude than that of $CuGaSe_2$, which frequently resulted in a segregation of Ga at CIGS/Mo interface in a two-step selenization processes [23,24]. This preferential reaction of In with Cu and Se will cause faster consumption of In to form $CuInSe_2$ than Ga, and consequently Ga may have relatively higher possibility to be removed in the form of Ga_2Se gas, which is thought to be a more probable reason for the Ga loss observed in this work. In addition, the Ga/III ratios of the final films, which are in a linear relationship with those of solutions, are thought to ensure the linearity of Cu/III ratios between the solution and final films (Fig. 3(a)). From these experimental results, it can be concluded that the addition of Ga–nitrate into the starting solution leads to better controllability of compositions compared to the CIS case, presumably by the competitive reactions between In and Ga to form Cu–III–Se_2 compounds.

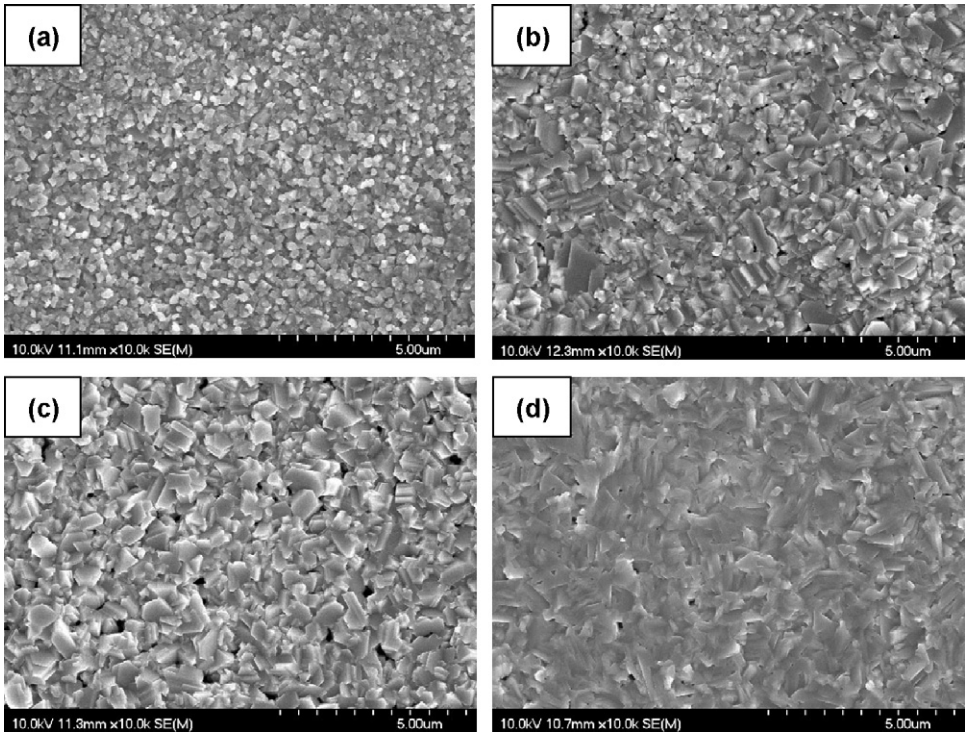

Fig. 4. Planar SEM micrographs of CIGS thin films with different Cu/III ratios of (a) 0.60, (b) 0.78, (c) 0.94 and (d) 1.17. Ga/III ratios of all the films were fixed to 0.17.

Previously, Kaelin et al. [6] reported that they observed a relative increase in Ga contents after selenization, which is opposite to our case. In the context of our hypothesis suggested above, we believe that this difference is originated from the different selenization conditions such as operating pressure or Se flux which definitely affect the tendency of the formation of Cu–III–Se compounds and re-evaporation of III_2Se gases.

3.3. Effects of Cu/III and Ga/III ratios on film properties

3.3.1. Cu/III ratios

Fig. 4 shows planar SEM micrographs of the selenized CIGS thin films with various Cu contents. Ga/III ratios of the films were fixed to 0.17. All the films show very dense and crack-free surface morphologies. The grain size was significantly influenced by Cu/III ratio, in which the higher was the Cu/III ratio the larger was the grain size. This is consistent with well-known effects of Cu-Se binary phase on the grain growth of CIGS films [25–27]. The Cu-Se phase is clearly seen in the XRD patterns of the films with Cu/III ratios over 1.17 (Fig. 5(a)). It is noticeable that (1 1 2) peaks of CIGS appear to shift to smaller angles as Cu/III ratio increases, as shown in the magnified view of (1 1 2) peaks (Fig. 5(b)). The peak shift is thought to be originated from the change in lattice parameter of chalcopyrite structure, but we cannot exclude the possibility of misunderstanding leaded by secondary phase related peak broadening.

To make this point clear, we performed Raman analysis on the CIGS films with different Cu contents (Fig. 5(c)) because the Raman shifts corresponding to chalcopyrite CIGS ($\sim$174 cm^{-1}), Cu–Se binary (260 cm^{-1}) and OVC phases (150 cm^{-1}) are easily distinguishable. In Fig. 5(c), it is clear that the A_1 mode frequency of chalcopyrite CIGS is systematically dependent on Cu contents. According to the relationship between the Raman spectra with local stress development [28], the increase in peak frequency is correlated with a compressive stress in a sample, reflecting a lattice compression with decrease in Cu contents in our case. This is well consistent with the XRD peak shifts shown in Fig. 5(b) in that the larger angle of (1 1 2) diffraction at lower Cu contents also means the smaller lattice constant. From these results, it was concluded that the Cu contents related peak shifts in XRD and Raman spectra are not secondary phase related, but are originated from the compression of chalcopyrite lattice itself presumably due to the development of point defects along with the change in Cu contents.

It has been well demonstrated that the favorable point defects in CIGS thin films are Cu vacancies (V_{Cu}) and antisite defects of In_{Cu}, and they can form in large concentrations of several percent [29–32]. Especially, the electrically neutral defect clusters of $2V_{Cu}$–In_{Cu} have particularly low formation energy, and they are considered to be the reason for the high compositional tolerance of $CuInSe_2$ compounds [30,32]. Rockett [31] further proposed that those defect clusters form larger structures ('superclusters') due to electrostatic interactions of individual defect cluster dipoles. To prevent the supercluster from having a net dipole, excess V_{Cu} can form around its perimeter, leading to no net dipole moment but a slight net negative charge [31]. As a consequence, as the material becomes increasingly Cu-poor the population of the defect clusters should also increase.

Considering that formation of these defect clusters require the removal of three monovalent copper ions and substitution on one of those vacancies of only one trivalent indium, significant lattice compression is expected. Consequently, the higher degree of lattice compression in Cu-poorer films is thought to be closely related to the more population of $2V_{Cu}$–In_{Cu} defect clusters. Another possible scenario is the lattice compression by individual V_{Cu} rather than by defect clusters. However, it cannot fully explain the composition dependent peak shifts shown in Fig. 5. For example, Cu-poorer films need less number of compensating V_{Cu} at the perimeter of defect clusters because the defect clusters are more closely packed by mutual electrostatic interaction [31]. In this case, the lattice compression due to the individual V_{Cu} should be mitigated as Cu contents decrease, which is opposite to our results. Accordingly,

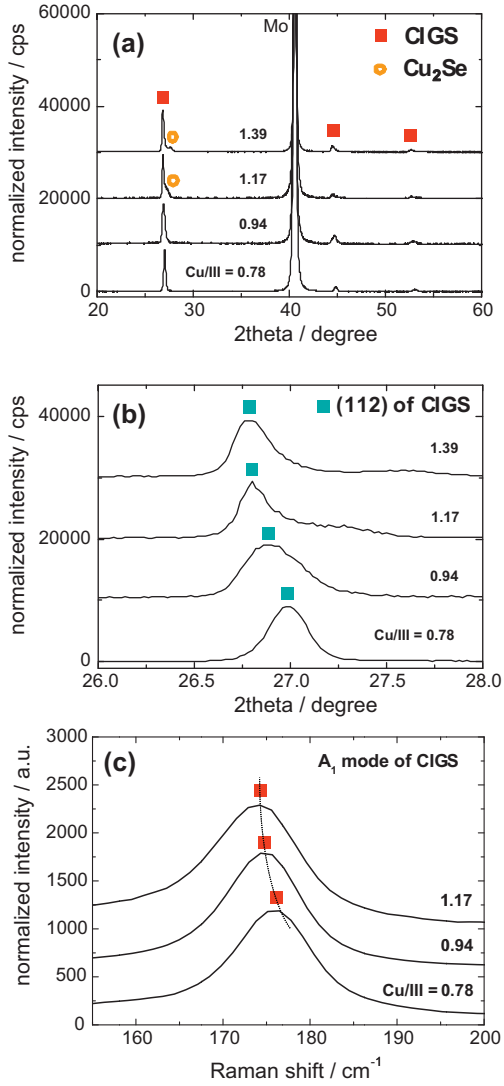

Fig. 5. (a) XRD patterns, (b) magnified view of Fig. 5(a) around (1 1 2) plane and (c) Raman spectra of the selenized films with different Cu/III ratios.

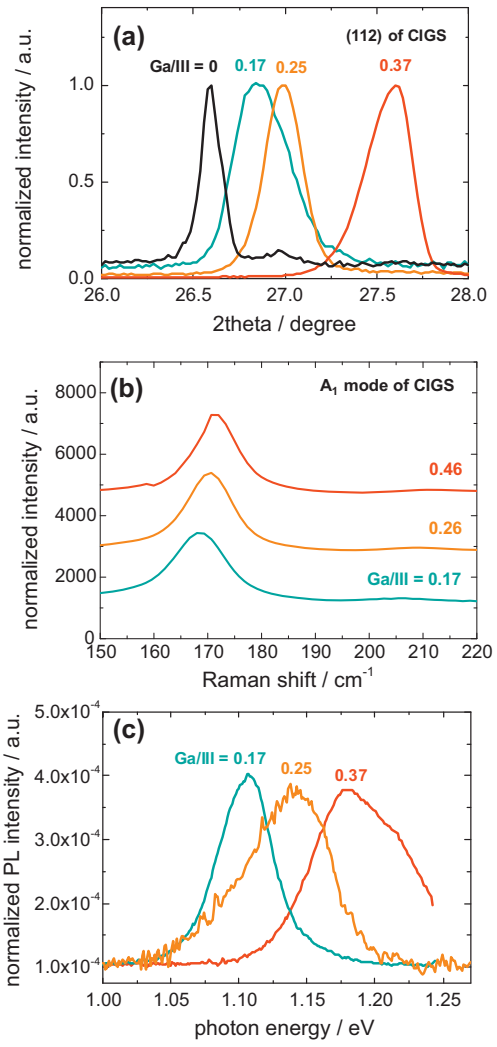

Fig. 7. Effects of Ga/III ratio of CIGS films on (a) XRD, (b) Raman and (c) PL spectra.

we argue that the formation of V_{Cu}–In_{Cu} defect superclusters in Cu-poor films is the reason of the XRD and Raman peak shifts shown in Fig. 5.

In order to investigate the effects of Cu/III ratios on optical properties of the films, PL spectra were obtained for samples with Cu/III = 0.65 and 0.94, and shown in Fig. 6. It is notable that PL intensity of the CIGS film with Cu/III = 0.65 is smaller than that of the film with Cu/III = 0.94 by a factor of 16, and energetic positions of dominant peaks are different between two samples, in which PL spectrum of Cu/III = 0.65 sample is dominated by two broad peaks positioned at 0.92 and 1.00 eV while that of Cu/III = 0.94 sample is by one intense peak at 1.11 eV. The general features of PL spectra shown in Fig. 6 are identical to those of co-evaporated CIS thin films reported by Zott et al. [33,34]. They found that for slightly In-rich composition (Cu/In = 0.95) the luminescence signal was typically dominated by a peak structured at about 0.94 eV whereas with decreasing Cu/In ratio the intensity of the emission line at 0.94 eV disappeared and other asymmetric broad lines appeared at lower energy positions around at 0.877 eV [34]. From the dependence of the transition energies of those peaks on excitation density, both the transitions were interpreted as donor-accepter pair (DAP) transitions [34]. Further, based on the fact that the same activation energy of about 40 meV was obtained for those two DAP transitions, they concluded that one defect (presumably the copper vacancies) participated in both emissions, and finally assigned the transition at higher energy as $V_{Se} \rightarrow V_{Cu}$ transition and that at lower energy as $In_{Cu} \rightarrow V_{Cu}$ transition [34]. Consequently, the peaks shown in Fig. 6 are also thought to be originated from the identical optical transitions, in which the peak at 1.11 eV of Cu/III = 0.94 samples is from DAP transition between V_{Cu} and V_{Se} and those at 1.0 and 0.92 eV of Cu/III = 0.65 sample, although clear distinguishment and descriptions on those two broad peaks are difficult at

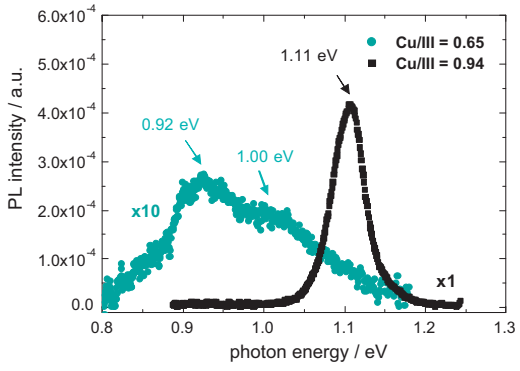

Fig. 6. PL spectra of CIGS thin films with Cu/III ratios of 0.65 and 0.94.

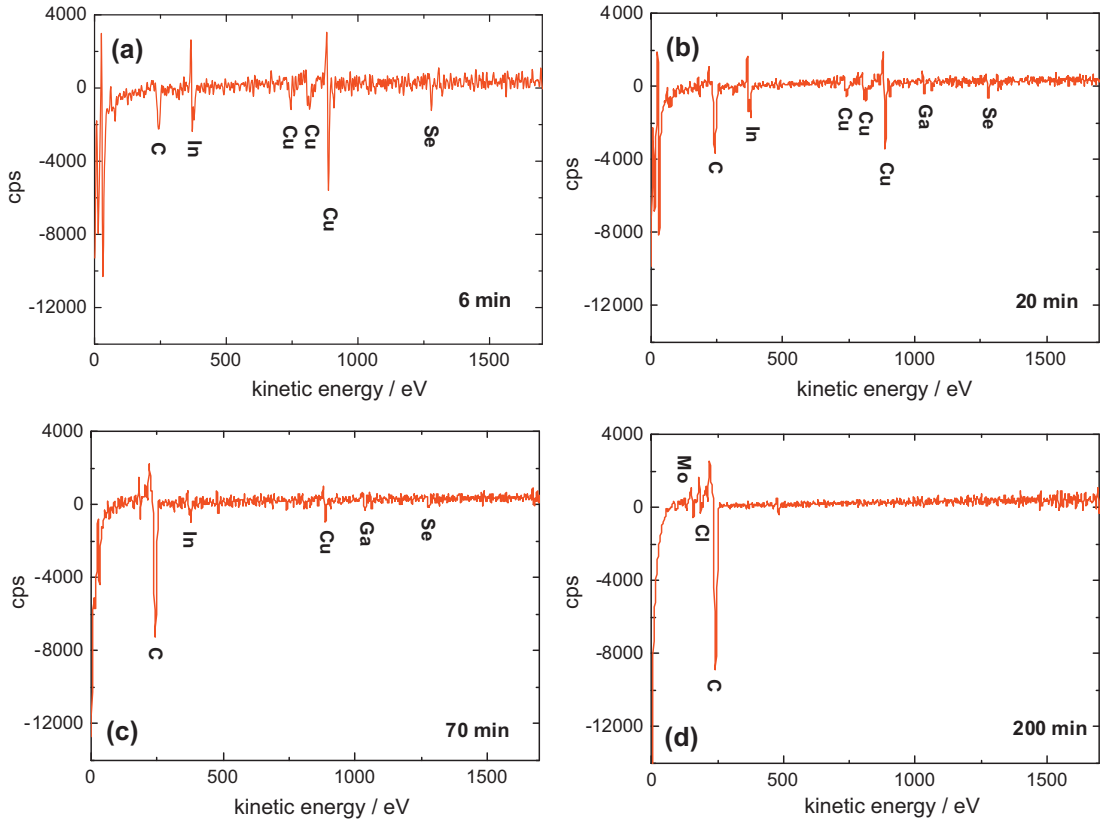

Fig. 8. AES scan profiles of CIGS/carbon film obtained after sputtering the sample for (a) 6 min, (b) 20 min, (c) 70 min and (d) 200 min.

this stage, are closely related to DAP transition between V_{Cu} and In_{Cu} defects. The difference between the absolute values of peak positions reported in reference 35 and in this work (for $V_{Se} \rightarrow V_{Cu}$ transition: 0.94 eV and 1.11 eV, respectively; for $In_{Cu} \rightarrow V_{Cu}$ transition: 0.877 eV and 1.0–0.92 eV, respectively) are attributed to the different Ga contents of the samples. These luminescence data are again well consistent with the peak shifts in XRD and Raman data (Fig. 5) in that the enhanced DAP transition between V_{Cu} and In_{Cu} at lower Cu/III ratio reflects the higher possibility to form such defect clusters.

3.3.2. Ga/III ratios

Fig. 7 shows the peak shift in (a) XRD, (b) Raman and (c) PL spectra according to Ga/III ratio of the CIGS thin films. Cu/III ratios of all the films were fixed to 0.94. It is easy to understand such shifts of characteristic peaks because addition of Ga, which has smaller ionic radius and atomic weight than In has, to replace In should definitely induce the compression of lattice, mass reduction and increase in bandgap of the films [35,36]. All of these features are well represented in our solution processed CIGS films (Fig. 7) with shifts of XRD peaks to higher diffraction angles, shifts of A_1 Raman mode to higher frequencies and shifts of PL peaks to higher energy positions with increasing Ga contents.

3.4. Bottom carbon layer

A critical issue on the bottom layer (Fig. 2(a)) is how electrical current flows through it. It is particularly important because films prepared by coating of pure EC/methanol solution were found to be electrical insulators. Previously, Kaelin et al. [6] stated that the bottom layer contains mainly carbon but there was no discussion about the electrical flow through the layer. On the other hand, Ahn et al. [7] suggested that current may flow by a conductive path embedded in carbon matrix formed by a connection of unreacted source materials, i.e., CuCl, In or Se. However, the possibility that carbon layer itself acts as a conductive path cannot be excluded. For the latter case, the structure of carbon should be changed by high temperature annealing (selenization) from an insulator to any type of electrically conductive form.

To get an answer to above question, we conducted AES analysis on the CIGS/carbon films. Fig. 8 shows AES scan profiles obtained at different sputtering time. It is clear that as sputtering time increases AES signals corresponding to Cu, In, Ga and Se gradually decrease. And after sputtering the sample for 200 min (Fig. 8(d)), those signals completely disappear. On the other hand, in Fig. 8(d), different AES signals corresponding to Mo and Cl are detected which are definitely originated from the back contact and the starting paste, respectively. The existence of Cl signal is interesting because Kealin et al. [6] and Ahn et al. [7] reported that no chlorine residual was detected in their EDS analyses. Fig. 8 reflects that in the top layer Cl was almost completely removed by evolution of Cl_2 gas as suggested by Ahn et al. [7], but the bottom layer still contained small amount of residual Cl embedded in carbon matrix.

However, regarding the current flow path through the bottom layer, it is not likely that Ahn's hypothesis works because the amount of Cl is too small for a connection of Cl residue to act as a main current flow route. Rather it is reasonable to consider that most electrical current flows through the carbon itself, and from the fact that there was no evidence of crystallization of carbon in the XRD and Raman data of our samples the carbon must be in a conductive amorphous state. Accordingly, the bottom layer should be regarded as a conductive amorphous carbon containing small amount of Cl residue.

4. Conclusion

Answers to the three questions about CIGS/carbon double layered films prepared by a direct coating approach of solution precursors can be summarized as follows;

(1) A better controllability of compositions of the final CIGS films, i.e., Cu/III and Ga/III ratios of the films, compared to the CIS case was confirmed, which is presumably due to the competitive reactions between In and Ga to form Cu–III–Se_2 compounds.
(2) Regarding the effects of Cu contents, systematic peak shifts in XRD and Raman spectra according to Cu/III ratio of the films were observed, and could be consistently interpreted by formation of V_{Cu}–In_{Cu} defect superclusters, which was further supported by the dependency of PL spectra of the films on Cu contents. Substitution of In by Ga also induced peak shifts in XRD, Raman and PL spectra, which was attributed to the mass and size difference between In and Ga.
(3) AES analysis revealed that the bottom layer was mostly composed of amorphous carbon without major sources materials of Cu, In, Ga and Se, reflecting that the main electrical current flow path is the amorphous carbon itself.

Acknowledgements

This study was partly supported by a grant from the cooperative R&D Program (B551179-08-03-00) funded by the Korea Research Council Industrial Science and Technology, Republic of Korea. This research was also partly supported by the Converging Research Center Program through the National Research Foundation of Korea (NRF) funded by the Ministry of Education, Science and Technology (2011K000579).

References

[1] I. Repins, M.A. Contreras, B. Egaas, C. DeHart, J. Scharf, C.L. Perkins, B. To, R. Noufi, Prog. Photovolt.: Res. Appl. 16 (2008) 235–239.
[2] C. Eberspacher, C. Fredric, K. Pauls, J. Serra, Thin Solid Films 387 (2001) 18–22.
[3] D.B. Mitzi, M. Yuan, W. Liu, A.J. Kellock, S.J. Chey, V. Deline, A.G. Schrott, Adv. Mater. 20 (2008) 3657–3662.
[4] M. Yuan, D.B. Mitzi, W. Liu, A.J. Kellock, S.J. Chey, V. Deline, Chem. Mater. 22 (2010) 285–287.
[5] T.T. John, M. Mathew, C.S. Kartha, K.P. Vijayakumar, T. Abe, Y. Kashiwaba, Sol. Energy Mater. Sol. Cells 89 (2005) 27–36.
[6] M. Kaelin, D. Rudmann, F. Kurdesau, H. Zogg, T. Meyer, A.N. Tiwari, Thin Solid Films 480–481 (2005) 486–490.
[7] S.J. Ahn, C.W. Kim, J.H. Yun, J.H. Gwak, S.H. Jeong, B.H. Ryu, K.H. Yoon, J. Phys. Chem. C 114 (2010) 8108–8113.
[8] V.K. Kapur, A. Bansal, P. Le, O.I. Asensio, Thin Solid Films 431–432 (2003) 53–57.
[9] D.L. Schulz, C.J. Curtis, R.A. Flitton, H. Weisner, J. Keane, R.J. Matson, K.M. Jones, P.A. Parilla, R. Noufi, D.S. Ginley, J. Electron. Mater. 27 (1998) 433–437.
[10] S.J. Ahn, K.H. Kim, Y.G. Chun, K.H. Yoon, Thin Solid Films 515 (2006) 4036–4040.
[11] S.J. Ahn, C.W. Kim, J.H. Yun, J.C. Lee, K.H. Yoon, Sol. Energy Mater. Sol. Cells 91 (2007) 1836–1841.
[12] S.J. Ahn, K.H. Kim, J.H. Yun, K.H. Yoon, J. Appl. Phys. 105 (2009) 113533–1113533.
[13] Q. Guo, G.M. Ford, H.W. Hillhouse, R. Agrawal, Nano Lett. 9 (2009) 3060–3065.
[14] Q. Guo, S.J. Kim, M. Kar, W.N. Shafarman, R.W. Birkmire, E.A. Stach, R. Agrawal, H.W. Hillhouse, Nano Lett. 8 (2008) 2982–2987.
[15] M.O. Lopez, A.M. Acevedo, Thin Solid Films 330 (1998) 96–101.
[16] M. Krunks, O. Bijakina, V. Mikli, H. Rebane, T. Varema, M. Altosaar, E. Mellikov, Sol. Energy Mater. Sol. Cells 69 (2001) 93–98.
[17] M. Krunks, O. Kijatkina, A. Mere, T. Varema, I. Oja, O. Milki, Sol. Energy Mater. Sol. Cells 87 (2005) 207–217.
[18] A. Parretta, M.L. Addonizio, S. Loreti, L. Quercia, M.K. Jayaraj, J. Cryst. Growth 183 (1998) 196–204.
[19] S. Jackson, B. Baron, R. Rocheleau, T. Russell, Am. Inst. Chem. Eng. J. 33 (1987) 711–721.
[20] A. Ludviksson, L.E. Rumaner, J.W. Rogers Jr., F.S. Ohuchi, J. Cryst. Growth 151 (1995) 114–120.
[21] V. Piacente, G. Bardi, V. Paolo Di, D. Ferro, J. Chem. Thermodynamics 8 (1976) 391–401.
[22] J.H. Greenberg, V.A. Borjakova, V.F. Shevelkov, J. Chem. Thermodynamics 5 (1973) 233–237.
[23] M. Marudachalam, R.W. BirkMire, H. Hichri, J.M. Schultz, A. Swartzlander, M.M. Al-Jassim, J. Appl. Phys. 82 (1997) 2896–2905.
[24] V. Alberts, Semicond. Sci. Technol. 19 (2004) 65–69.
[25] A. Rockett, F. Abou-Elfotouh, D. Albin, M. Bode, J. Ermer, R. Klenk, T. Lommasson, T.W.F. Russell, R.D. Tomlinson, J. Tuttle, L. Stolt, T. Walter, T.M. Peterson, Thin Solid Films 237 (1994) 1–11.
[26] R. Klenk, T. Walter, H.W. Schock, D. Cahen, Adv. Mater. 5 (1993) 114–119.
[27] K.H. Kim, K.H. Yoon, J.H. Yun, B.T. Ahn, Electrochem. Solid State Lett. 9 (2006) A382–A385.
[28] I.D. Wolf, Semicond. Sci. Technol. 11 (1996) 139–154.
[29] S.H. Wei, S.B. Zhang, A. Zunger, Appl. Phys. Lett. 72 (1988) 3199–3201.
[30] S.B. Zhang, S.H. Wei, A. Zunger, H. Katayama-Yoshida, Phys. Rev. B 57 (1998) 9642–9656.
[31] A. Rockett, Thin Solid Films 361–362 (2000) 330–337.
[32] S. Siebentritt, M. Igalson, C. Persson, S. Lany, Prog. Photovolt: Res. Appl. 18 (2010) 390–410.
[33] S. Zott, K. Leo, M. Ruckh, H.W. Schock, Appl. Phys. Lett. 68 (1996) 1144–1146.
[34] S. Zott, K. Leo, M. Ruckh, H.W. Schock, J. Appl. Phys. 82 (1997) 356–367.
[35] S. Theodoropoulou, D. Papadimitriou, N. Rega, S. Siebentritt, M.Ch. Lux-Steiner, Thin Solid Films 511–512 (2006) 690–694.
[36] J. Olejnicek, C.A. Kamler, A. Mirasano, A.L. Martinez-Skinner, M.A. Ingersoll, C.L. Exstrom, S.A. Darveau, J.L. Huguenin-Love, M. Diaz, N.J. Ianno, R.J. Soukup, Sol. Energy Mater. Sol. Cells 94 (2010) 8–11.